Available online at www.sciencedirect.com
ScienceDirect
Polyhedron 26 (2007) 1148–1158
POLYHEDRON
www.elsevier.com/locate/poly

Transition metal complexes with the quinolone antibacterial agent pipemidic acid: Synthesis, characterization and biological activity

Eleni K. Efthimiadou [a,b], Yiannis Sanakis [c], Nikos Katsaros [a], Alexandra Karaliota [b], George Psomas [a,*]

[a] Institute of Physical Chemistry, NCSR "Demokritos", GR-15310 Aghia Paraskevi Attikis, Greece
[b] Department of Inorganic Chemistry, Faculty of Chemistry, National and Kapodistrian University of Athens, Panepistimioupoli Zographou, GR-15701 Athens, Greece
[c] Institute of Materials Science, NCSR "Demokritos", GR-15310 Aghia Paraskevi Attikis, Greece

Received 29 August 2006; accepted 6 October 2006
Available online 19 October 2006

Abstract

Nine new mononuclear metal complexes of the quinolone antibacterial agent pipemidic acid (=HPPA) with VO^{2+}, Mn^{2+}, Fe^{3+}, Co^{2+}, Ni^{2+}, Zn^{2+}, MoO_2^{2+}, Cd^{2+} and UO_2^{2+} have been prepared and characterized with physicochemical and spectroscopic techniques. In all the complexes, pipemidic acid acts as a bidentate deprotonated ligand bound to the metal through the pyridone oxygen atom and one carboxylate oxygen atom. All the complexes are six-coordinate and the geometry round the metal atom can be described as a slightly distorted octahedron. For $VO(PPA)_2(H_2O)$, the axial position, *trans* to the vanadyl oxygen, is occupied by one pyridone oxygen atom. Molecular mechanics calculations in the gas state have been performed in order to propose a model for the structure of the Fe^{3+}, VO^{2+} and MoO_2^{2+} complexes. The antimicrobial activity of the complexes has been tested on three different microorganisms. The investigation with diverse spectroscopic techniques of the interaction of the complexes with calf-thymus DNA has shown that the complexes can be bound to DNA resulting in a B → A DNA transition.

Keywords: Pipemidic acid; Quinolones; Metal complexes; Spectroscopic study; Interaction with CT DNA; Antibacterial activity

1. Introduction

Study of the interaction between drugs and transition metals is an important and active research area in bioinorganic chemistry [1–4]. It is well known that the action of many drugs is dependant on the coordination with metal ions [1] or/and the inhibition [2] on the formation of metalloenzymes. Therefore, metal ions might play a vital role during the biological process of drug utilization in the body.

Quinolones, a commonly used term for the quinolonecarboxylic acids or 4-quinolones, are a group of synthetic antibacterial agents containing a 4-oxo-1,4-dihydroquinoline skeleton (Fig. 1a) [5]. They can act as antibacterial drugs that effectively inhibit DNA replication and are commonly used as treatment for many infections. Ciprofloxacin, cinoxacin, norfloxacin and nalidixic acid are among the most common and widely used quinolones.

The interaction of metal ions with diverse deprotonated quinolones as ligands has been thoroughly studied [5]. In the literature, there have been reported complexes of ciprofloxacin with $V(IV)O^{2+}$ [6], Fe(III) [7] and Cu(II) [8,9], complexes of cinoxacin with Co(II) [10], Ni(II) [11], Cu(II) [12,13], Zn(II) [11] and Cd(II) [14,15], of nalidixic acid with Zn(II) [16], of ofloxacin with Cu(II) [17] and two complexes of norfloxacin with Zn(II) [18]. There have also been reported mixed ligand copper(II) complexes of phenanthroline with nalidixic acid [19], cinoxacin [20] and ciprofloxacin [21] as well as ionic complexes of protonated norfloxacin with Zn(II) and Cu(II) [22], Cu(I) [23] and Mn [24]. For Mo only two cip-

* Corresponding author. Tel.:+30 2106503611; fax: +30 2106511766.
E-mail address: gpsomas@chem.demokritos.gr (G. Psomas).

0277-5387/$ - see front matter © 2006 Elsevier Ltd. All rights reserved.
doi:10.1016/j.poly.2006.10.017

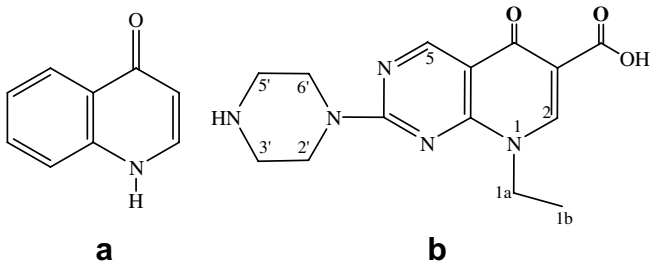

Fig. 1. (a) The 4-oxo-1,4-dihydroquinoline skeleton. (b) Pipedimic acid (8-ethyl-5,8-dihydro-5-oxo-2-(1-piperazinyl)pyrido(2,3-d)pyrimidine-6-carboxylic acid = HPPA) and atom labelling.

rofloxacin complexes as polyoxometalates have been characterized [25], while no quinolone complexes of $Mo(VI)O_2^{2+}$ and $U(VI)O_2^{2+}$ have been reported yet, although their role as bioelements is well established [26–29].

Pipemidic acid, HPPA (Fig. 1b), a 4-quinolone product, is an antibacterial agent used to treat gram-negative urinary tract infections [30] and severely damages DNA in the absence of an exogenous metabolizing system [31]. Pipemidic acid can act as a bidentate ligand through the quinolone oxygen and one carboxylate oxygen atom. In the literature, complexes of protonated pipemidic acid are reported with Ca^{2+}, Sr^{2+}, Ba^{2+}, Sn(IV) [32] and with the lanthanides La(III), Ce(III), Pr(III), Nd(III), Sm(III), Tb(III), Dy(III) and Y(III) [33] as well as of the deprotonated pipemidic acid with pentacoordinate Cu(II) and Mn(II) [34]. The reported results suggest that metal ion coordination might be involved in the antibacterial activity of HPPA [35].

We have initiated the study of the structure, spectroscopic and biological properties of transition metal complexes of diverse quinolone antibacterial drugs [36–39]. In this context we have studied the interaction of deprotonated pipemidic acid with the transition metal ions $V^{IV}O^{2+}$, Mn(II), Fe(III), Co(II), Ni(II), Zn(II),Cd(II), $Mo^{VI}O_2^{2+}$ and $U^{VI}O_2^{2+}$ in an attempt to examine the mode of binding and possible synergetic effects. The resulting mononuclear complexes have been characterized with elemental analysis and diverse spectroscopic techniques (IR, UV–Vis, NMR and EPR spectroscopy). Molecular modelling techniques have been employed so as to propose a low energy model for the most favorable isomer of the VO^{2+}, Fe^{3+} and MoO_2^{2+} complexes based on molecular mechanics calculations in the gas phase. The interaction of complexes with calf-thymus (CT) DNA has been studied with UV and circular dichroism (CD) spectroscopy. The antibacterial activity of the complexes has been also investigated against three microorganisms.

2. Experimental

2.1. Materials

All the chemicals for the synthesis of the compounds were used as purchased. DMF was distilled from calcium hydride (CaH_2) and CH_3OH from Mg, and stored over 3 Å molecular sieves. Diethyl ether, anhydrous grade and absolute ethanol were used without any further purification. Pipemidic acid and CT DNA were purchased from Sigma and $VOSO_4 \cdot 5H_2O$, $CoCl_2 \cdot 6H_2O$, $MnCl_2 \cdot 4H_2O$, $FeCl_3 \cdot 3H_2O$, $NiCl_2 \cdot 6H_2O$, $ZnCl_2$, $CdCl_2 \cdot 2.5H_2O$, $UO_2(NO_3)_2 \cdot 6H_2O$, $MoO_2(acac)_2$, KOH and all the solvents were purchased from Aldrich Co. Agarose was purchased from BRL. Tryptone and yeast extract were purchased from Oxoid (Unipath, Hampshire, UK). All chemicals and solvents were reagent grade.

DNA stock solutions (5 mM) were prepared by dilution of CT DNA with buffer (containing 150 mM NaCl and 15 mM trisodium citrate at pH 7.0) followed by exhaustive stirring at 4 °C for three days [40] and the solutions were kept at 4 °C for no longer than a week. The nucleotide concentrations were determined by their absorption at 260 nm using $\varepsilon = 6600\ M^{-1}\ cm^{-1}$ (expressed as phosphate).

2.2. Synthesis of the complexes

2.2.1. $VO(PPA)_2(H_2O)$ (1)

A warm methanolic solution (15 mL) of deprotonated pipemidic acid (0.4 mmol, 121 mg) was added to a methanolic solution (10 mL) of $VOSO_4 \cdot 5H_2O$ (0.2 mmol, 51 mg) and the reaction mixture was refluxed for 2 h. The solution was filtered and left for slow evaporation. After a few days a brown-green microcrystalline product was deposited, collected with filtration, washed with methanol and dried. Yield: 104 mg, ~75%. *Anal.* Calc. for $VO(PPA)_2(H_2O)$ ($C_{28}H_{34}N_{10}O_8V$) (MW = 689.58): C, 48.77; H, 4.97; N, 20.31. Found: C, 49.05; H, 5.03; N, 20.10%. The complex is soluble in DMSO and DMF and is a non-electrolyte.

In a similar way complexes **2**–**9** were prepared with the use of the corresponding metal salt.

2.2.2. $Mn(PPA)_2(H_2O)_2$ (2)

$MnCl_2 \cdot 4H_2O$ (0.2 mmol, 40 mg) was used. A yellow microcrystalline product was collected. Yield: 97 mg, ~70%. *Anal.* Calc. for $Mn(PPA)_2(H_2O)_2$ ($C_{28}H_{36}N_{10}O_8Mn$) (MW = 695.59): C, 48.35; H, 5.22; N, 20.13. Found: C, 48.62; H, 5.30; N, 19.89%. The complex is soluble in DMSO, DMF, CH_3CN and acetone and is a non-electrolyte.

2.2.3. $Fe(PPA)_3$ (3)

$FeCl_3 \cdot 3H_2O$ (0.2 mmol, 44 mg) and pipemidic acid (0.6 mmol, 192 mg) were used. An orange microcrystalline product was collected. Yield: 140 mg, ~67%. *Anal.* Calc. for $Fe(PPA)_3$ ($C_{42}H_{48}N_{15}O_9Fe$) (MW = 962.79): C, 52.39; H, 5.03; N, 21.82. Found: C, 51.93; H, 4.91; N, 22.03%. The complex is soluble in DMSO, DMF and H_2O and is a non-electrolyte.

2.2.4. $Co(PPA)_2(H_2O)_2$ (4)

$CoCl_2 \cdot 6H_2O$ (0.2 mmol, 48 mg) was used. An orange-yellow microcrystalline product was collected. Yield: 90 mg, ~65%. *Anal.* Calc. for $Co(PPA)_2(H_2O)_2$

($C_{28}H_{36}N_{10}O_8Co$) (MW = 699.59): C, 48.07; H, 5.18; N, 20.02. Found: C, 47.76; H, 5.37; N, 19.65%. The complex is soluble in DMSO and DMF and is a non-electrolyte.

2.2.5. $Ni(PPA)_2(H_2O)_2$ (5)

$NiCl_2 \cdot 6H_2O$ (0.2 mmol, 48 mg) was used. A light green microcrystalline product was collected. Yield: 98 mg, ~70%. *Anal.* Calc. for $Ni(PPA)_2(H_2O)_2$-($C_{28}H_{36}N_{10}O_8Ni$) (MW = 699.37): C, 48.09; H, 5.19; N, 20.03. Found: C, 48.41; H, 5.01; N, 20.17%. The complex is soluble in DMSO, DMF, ethanol and H_2O and is a non-electrolyte.

2.2.6. $Zn(PPA)_2(H_2O)_2$ (6)

$ZnCl_2$ (0.2 mmol, 28 mg) was used. A pale yellow microcrystalline product was collected. Yield: 105 mg, ~75%. *Anal.* Calc. for $Zn(PPA)_2(H_2O)_2$ ($C_{28}H_{36}N_{10}O_8Zn$) (MW = 706.04): C, 47.63; H, 5.14; N, 19.84. Found: C, 47.75; H, 5.21; N, 19.98%. The complex is soluble in DMSO, CH_3CN, acetone and H_2O and is a non-electrolyte.

2.2.7. $MoO_2(PPA)_2$ (7)

$MoO_2(acac)_2$ (0.2 mmol, 66 mg) was used. A pale yellow microcrystalline product was collected. Yield: 100 mg, ~69%. *Anal.* Calc. for $MoO_2(PPA)_2$ ($C_{28}H_{32}N_{10}O_8Mo$) (MW = 732.56): C, 45.91; H, 4.40; N, 19.12. Found: C, 46.19; H, 4.62; N, 19.00%. The complex is soluble in DMSO and DMF and is a non-electrolyte.

2.2.8. $Cd(PPA)_2(H_2O)_2$ (8)

$CdCl_2 \cdot 2.5H_2O$ (0.2 mmol, 46 mg) was used. A yellow microcrystalline product was collected. Yield: 100 mg, ~66%. *Anal.* Calc. for $Cd(PPA)_2(H_2O)_2$ ($C_{28}H_{36}N_{10}O_8Cd$) (MW = 753.07): C, 44.66; H, 4.82; N, 18.60. Found: C, 45.07; H, 4.75; N, 18.45%. The complex is soluble in DMSO, DMF, H_2O, $CHCl_3$ and acetone and is a non-electrolyte.

2.2.9. $UO_2(PPA)_2$ (9)

$UO_2(NO_3)_2 \cdot 6H_2O$ (0.2 mmol, 100 mg) was used. A pale yellow microcrystalline product was collected. Yield: 125 mg, ~70%. *Anal.* Calc. for $UO_2(PPA)_2$ ($C_{28}H_{32}$-$N_{10}O_8U$) (MW = 874.65): C, 38.45; H, 3.69; N, 16.01. Found: C, 38.88; H, 3.80; N, 15.87%. The complex is soluble in DMSO, DMF, CH_3CN, acetone and H_2O and is a non-electrolyte.

2.3. Physical measurements

IR spectra (400–4000 cm^{-1}) were recorded on a Nicolet Magna-IR 550 with samples prepared as KBr pellets. UV–Vis spectra were recorded on a Thermo Electron Corporation Helios α dual beam spectrophotometer. C, H, and N elemental analysis were performed on a Perkin–Elmer 240B elemental analyzer. Electric conductance measurements were carried out with a WTW model LF 530 conductivity outfit and a type C cell, which had a cell constant of 0.996. This represents a mean value calibrated at 25 °C with potassium chloride. NMR spectra were recorded with a Bruker Avance 500 MHz instrument and were processed by X-WIN NMR 2.6 (Bruker Analytik GmbH). X-band EPR spectra at liquid helium temperatures were recorded on a Bruker ER 200D EPR spectrometer equipped with an Oxford Instruments ESR900 cryostat and an Anritsu microwave frequency counter. Simulations of EPR spectra were carried out with a computer program written by Prof. Michael P. Hendrich, Department of Chemistry, Carnegie Mellon University, Pittsburgh, USA [41,42].

All CD spectra were recorded on a Jasco J-700 spectropolarimeter using a 1.0 cm path quartz cell and the following acquisition parameters: $\lambda = 190$–400 nm, scan speed 50 nm min^{-1}, resolution step 0.2 nm, sensitivity 50 mdeg, response 1 s, bandwidth 1.0 nm, accumulations 10. In some cases, the spectra were averaged over an appropriate number of scans. All CD spectra were recorded at 25 °C after the complexes had been incubated with CT DNA for 24 h at 37 °C.

2.4. Molecular modelling

With the aim to present a molecular model for each new complex that is unbiased by the starting structure, we have used Langevin dynamics with a simulated annealing protocol. Using this method, the mean total energy of an ensemble of structures guides the selection of the most favorable configuration for each complex. The starting structures were constructed using the program HyperChem and the MM+ force field that is based on the Allinger's MM2 force field [43]. For all the metal ions we used a default parameter set with $R^* = 2.20$ Å and $e^* = 0.02$ kcal mol^{-1}, since their van der Waals interactions are not expected to play a major role in such bonded representations as in octahedral complexes. Metal–ligand bond lengths were corrected in the final models using harmonic restraints with equilibrium values that were extracted from crystallographic data of similar compounds [44–56] (Tables S1, S3, and S5). Non-bonded interactions were calculated in vacuo with no cutoff and the electrostatic energy term was treated using bond dipoles. Initial energy minimizations were carried out by a conjugate gradient method with rms gradient <0.01 as convergence criterion.

Each model (Schemes S1–S3) was subjected to 20 individual rounds of simulated annealing setting a different value to the seed for the assignment of the starting velocities. To integrate the Langevin equation [57] the step size was set to 1fs and the collision frequency to 1 ps^{-1}. The annealing calculation comprised three phases: (i) raising the temperature of the system from 10 to 1000 K over 2 ps, (ii) keeping the system at 1000 K for 3 ps, and (iii) cooling the system down to 0 K over 15 ps. A tight coupling of the system with temperature (0.1 ps) was used for the heating and equilibration

phases. During the cooling phase the bath relaxation time was gradually decreased from 5.0 ps (7000 steps), 2.0 ps (3000 steps), 1.0 ps (2000 steps), 0.5 ps (2000 steps) to 0.05 ps (1000 steps). At the final step all structures had rms gradient < 0.01 and their total energy was recorded (Tables S2, S4, and S6). The models presented herein were selected from among the lowest energy structures that were generated for each starting geometry. A final minimization of their energy was performed as above, but having applied the metal–ligand distance restraints.

2.5. Antibacterial activity – minimum inhibitory concentration

The antibacterial activity of the compounds (ligands, metal salts and complexes) was studied against *S. aureus*, *E. coli* and *P. aeruginosa*. The microorganisms were maintained in the laboratory of "Inorganic Materials and Biomolecules" of NCSR "Demokritos". Screening was performed by determining the minimum inhibitory concentration (MIC). Two different media [Luria broth medium (=LB, containing 1% w/v tryptone, 0.5% w/v NaCl and 0.5% w/v yeast extract) and minimal medium salts broth (=MMS, containing 1.5% w/v glucose, 0.5% w/v NH_4Cl, 0.5% w/v K_2HPO_4, 0.1% w/v NaCl, 0.01% w/v $MgSO_4 \cdot 7H_2O$ and 0.1% w/v yeast extract)] were used. The compounds were dissolved in distilled water with twofold serial dilutions from 128 to 4 $\mu g\,mL^{-1}$. All cultures were incubated at 37 °C. Control tests with no active ingredients were also performed.

The MIC was determined using twofold serial dilutions in liquid media containing 4–128 $\mu g\,mL^{-1}$ of the compound being tested. The solvent used was water where the solubility of the compound permits and DMSO in the remaining cases. The activity of DMSO has been also investigated and no activity at the quantities used in this work has been found. A preculture of bacteria was grown in LB overnight at the optimal temperature of each species. Two milliliters of MMS were inoculated with 20 mL of this preculture. This culture was used as a control to examine if the growth of the bacteria tested is normal. In a similar second culture, 20 μL of the bacteria as well as the tested compound at the desired concentration were added. A third sample containing 2 mL MMS supplemented with the same compound concentration was used as a second control to check the effect of the compound on MMS. All samples were in duplicate. We monitored bacterial growth by measuring the turbidity of the culture after 12 and 24 h. If a certain concentration of a compound inhibited bacterial growth, half the concentration of the compound was tested. This procedure was carried on to a concentration that bacteria grow normally. The lowest concentration that inhibited bacterial growth was determined as the MIC value. All equipment and culture media were sterile.

3. Results and discussion

3.1. Synthesis of the complexes

All the complexes have been prepared at high yield (65–75%) via the addition of a methanolic solution of deprotonated pipemidic acid to a methanolic solution of the metal ion at a ratio 3:1 for Fe^{3+} and 2:1 for the remaining divalent metal ions according to the reaction:

$$M^{n+} + n\mathrm{PPA} \rightarrow M(\mathrm{PPA})_n(H_2O)_x$$

where $M^{n+} = VO^{2+}$, Mn^{2+}, Co^{2+}, Ni^{2+}, Zn^{2+}, MoO_2^{2+}, Cd^{2+}, UO_2^{2+} ($n = 2$) and Fe^{3+} ($n = 3$), $x = 0$, 1 or 2. All complexes were collected as microcrystalline products. Although diverse crystallization techniques were employed, we did not manage to obtain crystals suitable for determination of structures with X-ray crystallography.

3.2. Infrared spectroscopy

In Table 1 the characteristic absorptions of the IR spectra of all the complexes are listed. In the IR spectra of complexes **1**–**9** the band at 1723 cm^{-1} in the HPPA spectrum attributed to the absorption of $\nu(C{=}O)_{carb}$ has disappeared and has been replaced by two very strong characteristic bands in the ranges 1600–1615 cm^{-1} and 1370–1360 cm^{-1}, that can be assigned as asymmetric, $\nu(CO_2)_{asym}$, and symmetric, $\nu(CO_2)_{sym}$, stretching ν(O–C–O) vibrations. The difference $\Delta = \nu_{asym}(CO_2) - \nu_{sym}(CO_2)$ is a useful characteristic for determining the coordination mode of the ligands. The Δ values fall in the range 238–252 cm^{-1}, indicating a monodentate coordination mode of the carboxylato group [58–60]. Finally, the pyridone stretch $\nu(C{=}O)_p$ is shifted from 1617 to 1634 cm^{-1} upon bonding. These changes of the IR spectra suggest that PPA is coordinated to the metal via the pyridone oxygen and one carboxylate oxygen atom [5].

The existence and the number of the $\nu(M{=}O)$ absorptions is a useful diagnostic tool of complex characterization. The appearance of the V=O stretching frequency in complex **1** at ~954 cm^{-1} suggests that a monoanionic ligand lies in a *trans* position to O_v ($O_{vanadyl}$) [61]. This acceptance is indicative of the arrangement of one O_{carb} ($O_{carboxylate}$) or O_{pyr} ($O_{pyridone}$) atom in the axial position of the octahedron around the V atom and excludes the O_w (O_{water}) atom. The existence of two $\nu(M{=}O)$ absorptions for MoO_2^{2+} and UO_2^{2+} complexes are indicative of a *cis* arrangement of two oxygen atoms around Mo and U atoms, respectively [26]. The band at ~3400–3420 cm^{-1} in the IR spectra of the complexes **1**, **2**, **4**, **5**, **6** and **8** can be attributed to the ν(O–H) vibration of one or two coordinated water molecules [59].

3.3. Electronic spectroscopy

The UV–Vis spectra of the complexes have been recorded as nujol mulls and in solution. The solvent has

Table 1
Characteristic absorptions (in cm^{-1}) of the IR spectra of the complexes

	$\nu(C{=}O)_p$	$\nu(CO_2)_{asym}$	$\nu(CO_2)_{sym}$	Δ[a]	$\nu(M=O)$
HPPA	1617	1723[b]			
$VO(PPA)_2(H_2O)$	1629	1606	1368	238	950
$Mn(PPA)_2(H_2O)_2$	1634	1608	1362	246	
$Fe(PPA)_3$	1637	1615	1363	252	
$Co(PPA)_2(H_2O)_2$	1625	1604	1362	242	
$Ni(PPA)_2(H_2O)_2$	1628	1608	1361	247	
$Zn(PPA)_2(H_2O)_2$	1626	1609	1362	247	
$MoO_2(PPA)_2$	1625	1603	1365	238	930, 900
$Cd(PPA)_2(H_2O)_2$	1624	1605	1360	245	
$UO_2(PPA)_2$	1634	1614	1365	249	910, 870

[a] $\Delta = \nu(CO_2)_{asym} - \nu(CO_2)_{sym}$.
[b] As ν(COOH).

been chosen based on the solubility of each complex. Practically, the spectra in solution are identical with those in nujol with the exception of a few nm shifts in some cases. In Table 2, the UV–Vis spectral data of all the complexes in the different solvents are given.

The UV spectra of the complexes are practically identical with that of the pipemidato ligand but slightly shifted, indicative of coordination through the pyridone and one carboxylate oxygen atom.

In the visible spectra, there are characteristic bands attributed to d-d transitions only for VO^{2+}, Fe^{3+}, Co^{2+} and Ni^{2+} complexes. For the $V^{IV}O^{2+}$ complex three low-intensity bands at ~802 (band I), 600 (band II) and 495 (band III) nm attributed to d–d transitions are observed. Band I at $\lambda = 802$ nm ($\varepsilon = 12\ M^{-1}\ cm^{-1}$) can be attributed to a $b_2(d_{xy}) \rightarrow e^*_\pi(d_{xz}, d_{yz})$ transition of the $V^{IV}O^{2+}$ and band II at $\lambda = 600$ nm ($\varepsilon = 20\ M^{-1}\ cm^{-1}$) to a $b_2(d_{xy}) \rightarrow b_1^*(d_{x^2-y^2})$ transition [62]. Band III at $\lambda = 495$ nm ($\varepsilon = 26\ M^{-1}\ cm^{-1}$) is also observed and can be attributed to a $d_{xy} \rightarrow d_{z^2}$ transition, although it usually lies under the much stronger ligand-to-metal charge-transfer (=LMCT) transition at $\lambda = 425$ nm ($\varepsilon = 100\ M^{-1}\ cm^{-1}$) and can be difficult to distinguish [63,64]. These bands are typical for distorted octahedral VO^{2+} complexes [46,48,61].

The spectrum of $Fe(PPA)_3$ exhibits two bands that can be attributed to d–d transitions: one weak band (as a shoulder) at ~600 nm ($\varepsilon = 30\ M^{-1}\ cm^{-1}$) which can be assigned as a $^6A_{1g} \rightarrow {}^5T_{1g}$ transition and an intense one at $\lambda = 500$ nm ($\varepsilon = 95\ M^{-1}\ cm^{-1}$) assigned as a $^6A_{1g} \rightarrow T_{2g}(G)$ transition [65,66]. These bands are typical for distorted octahedral Fe^{3+} complexes [49–51]. Additionally, a band at $\lambda = 436$ nm ($\varepsilon = 135\ M^{-1}\ cm^{-1}$), observed as a shoulder, can be attributed to a LMCT transition.

In the visible spectra of $Co(PPA)_2(H_2O)_2$ and $Ni(PPA)_2(H_2O)_2$ one band at ~555 ($\varepsilon = 40\ M^{-1}\ cm^{-1}$) and ~625 nm ($\varepsilon = 45\ M^{-1}\ cm^{-1}$), respectively, attributed to a d–d transition has been found as expected for octahedral Co^{2+} [67] and Ni^{2+} [68] high-spin complexes. Similar behavior has been observed for the octahedral high-spin Co^{2+} [12] and Ni^{2+} [11] cinoxacin complexes.

All the complexes also exhibit an absorption band at ~425–435 nm which can be assigned to the LMCT transition for the quinolone ligand [36–39].

3.4. NMR spectroscopy

^1H NMR spectra of HPPA, $Zn(PPA)_2(H_2O)_2$ and $UO_2(PPA)_2$ have been recorded in d_6-DMSO. The assignment of every signal has been achieved by comparing the

Table 2
Characteristic bands λ_{max} (nm) (ε, $M^{-1}\ cm^{-1}$) in the UV–Vis spectra of the complexes in different solvents

	IL bands		Band CT	Bands d–d		
HPPA[a]	330 (1900)	359 (1350)				
$VO(PPA)_2(H_2O)$[a]	331 (2200)	370 (1350)	425(sh)[d] (100)	495(sh) (26)	600 (20)	802 (12)
$Mn(PPA)_2(H_2O)_2$[a]	332 (2250)	370 (1230)	425(sh) (135)			
$Fe(PPA)_3$[b]	329 (2400)	375 (1250)	436(sh) (135)	500 (95)	600 (30)	
$Co(PPA)_2(H_2O)_2$[c]	327 (2150)	368 (1430)	425(sh) (120)		555 (40)	
$Ni(PPA)_2(H_2O)_2$[c]	342 (2350)	372 (1180)	430(sh) (125)		625 (45)	
$Zn(PPA)_2(H_2O)_2$[c]	330 (2150)	369 (1190)	425(sh) (145)			
$MoO_2(PPA)_2$[a]	329 (2150)	370 (1420)	423(sh) (115)			
$Cd(PPA)_2(H_2O)_2$[a]	334 (2350)	370 (1450)	420(sh) (145)			
$UO_2(PPA)_2$[a]	342 (1780)	368 (1380)	422(sh) (120)			

[a] In DMSO.
[b] In H_2O.
[c] In DMF.
[d] (sh) = shoulder.

^{1}H NMR spectra of the complexes to that of the ligand and spectra reported in the literature [69]. The results are shown in Table 3.

Comparison of the ^{1}H NMR spectra of $Zn(PPA)_2(H_2O)_2$ and $UO_2(PPA)_2$ with that of HPPA shows a significant perturbation of the chemical shift (up to 0.7 ppm) of the aromatic protons H2 and H5, indicating that H2 and H5 are close to the coordination site of the ligand. The signals for the aliphatic and piperazine protons are practically unchanged since they lie far from the binding site of the ligand.

The overall changes of the NMR spectra of the complexes are indicative of coordination of the pipemidato ligand to the metal via the pyridone and carboxylate oxygen atoms.

3.5. EPR spectroscopy

The EPR spectrum of $VO(PPA)_2(H_2O)$ in DMSO at 12 K is shown in Fig. 2. The spectrum is typical for a mononuclear VO^{2+} complex. We have simulated the spectrum assuming an $S = 1/2$ species interacting with a nucleic spin of $I = 7/2$ through the usual spin Hamiltonian:

$$H = \beta \mathbf{SgB} + \mathbf{IAS}$$

where β is the Bohr magneton and **A** is the tensor of the hyperfine interaction. The spectrum is well reproduced with axial **g**- and **A**-tensors with the values $g_{\|}$=1.942(2), $g_{\perp} = 1.976(2)$, $g_{iso} = (2g_{\perp} + g_{\|})/3 = 1.965$, $A_{\|} = 170(1) \times 10^{-4}$ cm^{-1}, $A_{\perp} = 59.7(1) \times 10^{-4}$ cm^{-1} and $A_{iso} = (2A_{\perp} + A_{\|})/3 = 96.5 \times 10^{-4}$ cm^{-1}. The experimentally deduced pair of values ($g_{\|} = 1.942(2)$ and $A_{\|} = 170(1) \times 10^{-4}$ cm^{-1}) support an O_4 basal plane of the octahedron [60].

The value of $A_{\|}$ is helpful in predicting the nature of the equatorial ligands of the VO^{2+} moiety through the "additivity principle" [70–72]. In the present case, the ligands involved are two O_{carb} and two O_{pyr} atoms of PPA ligands and one O_w atom. From the literature we obtained $A_{\|}(O_{pyr}) = 38.6 \times 10^{-4}$ cm^{-1}, $A_{\|}(O_{carb}) = 42.7 \times 10^{-4}$ cm^{-1} and $A_{\|}(O_w) = 45.7 \times 10^{-4}$ cm^{-1} [71,72]. By making use of these values, the three possible configurations and the respective $A_{\|}$ values are: (i) two O_{carb} and two O_{pyr} atoms of PPA with O_w at the axial position and $A_{\|} = 162.6 \times 10^{-4}$ cm^{-1}, (ii) two O_{pyr}, one O_{carb} atoms of PPA and one O_w with the other O_{carb} at the axial position and $A_{\|} = 165.6 \times 10^{-4}$ cm^{-1} and (iii) two O_{carb}, one O_{pyr} atoms of PPA and one O_w with the other O_{pyr} at the axial position and $A_{\|} = 169.7 \times 10^{-4}$ cm^{-1}. We observe that the configuration with an axial O_w gives rise to a relatively low $A_{\|}$ value in comparison to the experimental value of $A_{\|} = 170(1) \times 10^{-4}$ cm^{-1}, suggesting that O_w occupies an equatorial position, lying *cis* to O_v. Among the other two configurations, the conformation with O_{pyr} at the axial position is more consistent with the EPR parameters and in agreement with that observed in the crystal structure of the complex VO(ciprofloxacinato)$_2$(H_2O) [45] where $A_{\|} = 173 \times 10^{-4}$ cm^{-1}, leading us to the conclusion that the equatorial sites of the octahedron around V are occupied by two O_{carb} and one O_{pyr} atoms of PPA ligands and one O_w, with the second O_{pyr} at the axial position *trans* to O_v.

The EPR spectrum of $Fe(PPA)_3$ in DMSO at 12 K shows a signal at $g \sim 4.3$, characteristic for a high-spin Fe^{3+} ion in an almost rhombic environment. The EPR spectrum of $Mn(PPA)_2(H_2O)_2$ in DMSO consists of a six line pattern at $g \sim 2.0$, typical for a mononuclear Mn^{2+} ($S = 5/2$) complex. The EPR spectrum of $Co(PPA)_2(H_2O)_2$ in DMF at 10 K is rather complicated; it exhibits multiple signals, has a maximum at $g \sim 5.7$ and is consistent for a mononuclear octahedral high-spin Co^{2+} ($S = 3/2$) complex.

Table 3
Chemical shifts (ppm) in ^{1}H NMR spectra of HPPA, $Zn(PPA)_2(H_2O)_2$ and $UO_2(PPA)_2$ in d_6-DMSO

	HPPA	$Zn(PPA)_2(H_2O)_2$	$UO_2(PPA)_2$
H2 and H5	8.90 (2H)	8.16 (2H)	8.16 (2H)
H1a	4.39 (2H)	4.39 (2H)	4.40 (2H)
H1b	1.36 (3H)	1.35 (3H)	1.35 (3H)
H2′, H6′ or	3.14–3.25 (4H)	3.15–3.23 (4H)	3.15–3.26 (4H)
H3′, H5′	3.86(4H)	3.81(4H)	3.70 (4H)
H4′	9.19 (1H)	8.91 (1H)	8.91 (1H)

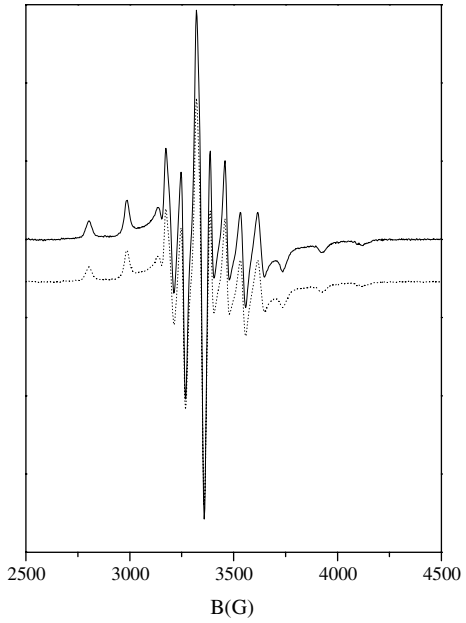

Fig. 2. Experimental (——) and theoretical (·····) EPR spectrum for complex $VO(PPA)_2(H_2O)$ in DMSO. EPR conditions: $T = 12$ K; microwave power = 0.13 mW; modulation amplitude = 5 Gpp; microwave frequency = 9.42 GHz.

3.6. Molecular dynamics

3.6.1. $Fe(PPA)_3$

In order to present a model for the complex we have constructed the two *fac*- and the two *mer*-$Fe(PPA)_3$

enantiomers (Scheme S1). The average energy of each set of enantiomers is almost equal, as is expected from such molecular mechanics calculations. However, the final structures of *mer*-[Fe(PPA)$_3$] exhibit lower energies by less than 0.3 kcal mol^{-1} in comparison to the energies of the *fac* isomers. For the *mer* models we have applied a set of harmonic restraints at the metal–ligand bonds during an additional minimization phase (Table S1) [49–52]. Based on these results we present the lowest energy model of one *mer*-[Fe(PPA)$_3$] enantiomer as the favorable configuration of the complex (Fig. S1). However, we can neither exclude the formation of any of the other isomers, nor unambiguously distinguish between the favorable enantiomers.

3.6.2. VO(PPA)$_2$(H$_2$O)

Using the same approach as above, 8 diastereoisomers of the VO(PPA)$_2$(H$_2$O) complex have been constructed (Scheme S2). In all these models the water molecule occupies a *cis* position with respect to V = O, in accordance with our EPR results and just as in similar vanadyl complexes [45–48]. Again, the resultant models of all VO(PPA)$_2$(H$_2$O) isomers exhibit comparable average total energy with the two *transOc* enantiomers (as are arbitrarily designated in Scheme S2) being more stable by more than 2 kcal mol^{-1} (Table S4). After application of the distance restraints to the M–L bonds (Table S3) and their geometry correction by minimizing the energy of the complex, the structure of the predicted most stable isomer is obtained (Fig. 3).

3.6.3. MoO$_2$(PPA)$_2$

Three pairs of enantiomers have been constructed as starting models of MoO$_2$(PPA)$_2$ (Scheme S3). After the Langevin dynamics simulated annealing calculations, we obtained the total energy results of 20 different conformations for each starting model, which guide us to select the *transOc* isomers as the more favorable. Their average energy is almost equal, as expected, and is lower than the other four isomers by more than 3 kcal mol^{-1} (Table S6). The lowest energy model structure found is illustrated in Fig. S3.

3.7. Antimicrobial activity

The efficiencies of the complexes have been tested against two Gram(−), *Escherichia coli* (*E. coli*) and *Pseudomonas aeruginosa* (*P. aeruginosa*), and one Gram(+), *Staphylococcus aureus* (*S. aureus*), microorganisms. The results are presented in Table 4.

It is evident (Table 4) that the ligand and the complexes have inhibitory action against all microorganisms tested and the coordination of HPPA (MIC = 16–64 μg mL^{-1}) with transition metal ions results in diverse biological activity (MIC for the complexes = 8–64 μg mL^{-1}). The activity of complexes VO(PPA)$_2$(H$_2$O), Mn(PPA)$_2$(H$_2$O)$_2$, MoO$_2$(PPA)$_2$ and Cd(PPA)$_2$(H$_2$O)$_2$ is equal to that of HPPA against all microorganisms tested. Complexes Fe(PPA)$_3$

Table 4
MIC in μg mL^{-1}

	E. coli	*P. aeruginosa*	*S. aureus*
HPPA	64	64	16
VO(PPA)$_2$(H$_2$O)	64	64	16
Mn(PPA)$_2$(H$_2$O)$_2$	64	64	16
Fe(PPA)$_3$	64	64	32
Co(PPA)$_2$(H$_2$O)$_2$	64	64	32
Ni(PPA)$_2$(H$_2$O)$_2$	64	32	32
Zn(PPA)$_2$(H$_2$O)$_2$	32	32	32
MoO$_2$(PPA)$_2$	64	64	16
Cd(PPA)$_2$(H$_2$O)$_2$	64	64	16
UO$_2$(PPA)$_2$	8	8	8

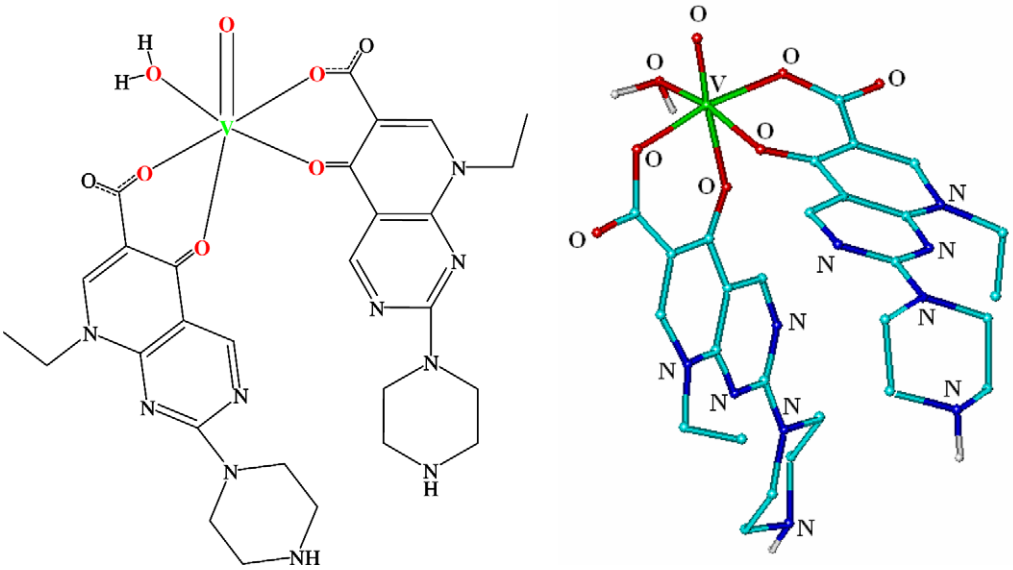

Fig. 3. Lowest energy model of VO(PPA)$_2$(H$_2$O).

and $Co(PPA)_2(H_2O)_2$ have antibacterial activity against *E. coli* and *P. aeruginosa* similar to that of HPPA (MIC = 64 μg mL^{-1}), but they are twice less active against *S. aureus* (MIC = 32 μg mL^{-1}). The antibacterial activity of $Ni(PPA)_2(H_2O)_2$ against *E. coli* is equal to that of HPPA. $Ni(PPA)_2(H_2O)_2$ is twice more active than HPPA against *P. aeruginosa* and twice less active against *S. aureus*. $Zn(PPA)_2(H_2O)_2$ is twice more active than HPPA against two Gram(−) microorganisms but twice less active against *S. aureus*. Finally, $UO_2(PPA)_2$ is four and two times more active than HPPA against two Gram(−) microorganisms and *S. aureus*, respectively.

The antimicrobial activity of the metal salts has also been investigated. It has been found that the metal salts do not exhibit antimicrobial activity at the concentration range used to assay the activity of the complexes in this work. When the antimicrobial activity of the metal complexes is investigated, the following principal factors [73,74] should be considered: (i) the chelate effect of the ligands; (ii) the nature of the *N*-donor ligands; (iii) the total charge of the complex; (iv) the existence and the nature of the ion neutralizing the ionic complex; (v) the nuclearity of the metal center in the complex. For complexes **1**–**9**, only the first of these factors is present, i.e. the chelate effect of the ligand. This is probably one of the main reasons for the diverse antibacterial activity shown by the complexes while the nature of the metal ion coordinated to PPA may have a significant role in this diversity. The significant improvement of the activity of PPA when coordinated to the uranyl complex is simply an evidence of the role of the coordinated metal ion [45]. On the other hand, further biological experiments in order to clarify the possible mechanism of action of the complexes are under investigation.

In conclusion, the best inhibition of the complexes is provided by $UO_2(PPA)_2$ (MIC = 8 μg mL^{-1}) against the three microorganisms tested.

3.8. Interaction of the complexes with CT DNA

DNA can provide three distinctive binding sites for the quinolone complexes; namely, groove binding, binding to phosphate group and intercalation [75]. This behavior is of great importance with regard to the relevant biological role of fluoroquinolone antibiotics in the human body [76,77].

3.8.1. Study of the complexes – CT DNA interaction with UV spectroscopy

The absorption spectra of the interaction of the complexes with CT DNA have been recorded for a constant CT DNA concentration (3.125×10^{-4} M) in different mixing ratios. Representative UV spectra of the complexes **1**, **2** and **9** with CT DNA derived for diverse complex:CT DNA mixing ratios (*r*) are shown in Fig. 4 while UV spectra of all the complexes with CT DNA are shown in Fig. S4. The changes observed in the absorption spectra

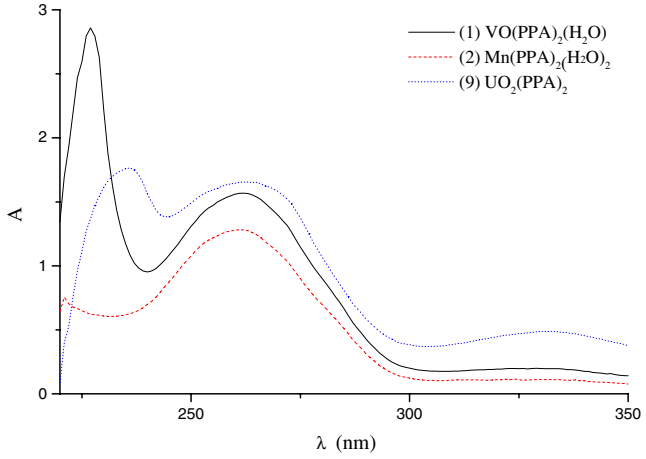

Fig. 4. Absorption spectra of complexes **1**, **2** and **9** in the presence of CT DNA. The *r* value is 1:200. The spectra were recorded at 25 °C after complexes had been incubated with CT DNA for 24 h at 37 °C.

of the complexes after mixing with CT DNA indicate that the interaction of the complexes with CT DNA takes place by a direct formation of a new complex with double-helical CT DNA [78].

3.8.2. Study of the complexes – CT DNA interaction with CD spectroscopy

The CD spectra of the complexes with double-stranded CT DNA for different *r* values can provide us with useful information concerning the complex–nucleotide interaction. The CD spectra of the interaction of the free ligand with CT DNA do not show any transitions because there is not any asymmetry or chirality in the molecules [78].

The CD spectrum of free CT DNA is conservative and consists of a negative band at 245 nm and a positive one at 275 nm, characteristic of the B-form of DNA [79]. The CD spectra of CT DNA in the presence of complex **1** are shown in Fig. 5a. They consist of a positive band I at 275 nm and a strong negative one II at 246 nm. When *r* increases, the λ_{max} of band I is shifted from 275 nm to higher wavelengths (up to 282 nm) followed by a decrease of the intensity, indicating that the DNA-form changes from the B- to A-form (B → A transition). This change (CD Cotton effect) is characteristic of reduced DNA helicity which is attributed to complex interstrand crosslinking to the DNA pairs [80]. Quite similar behavior is observed in the CD spectra of CT DNA in the presence of complex $MoO_2(PPA)_2$.

The CD spectra of CT DNA in the presence of complex **2** are shown in Fig. 5b. The increase of *r* leads to a raise in the intensity of band I at 275 nm and a shift of the λ_{max} from 280 nm to lower wavelengths (up to 274 nm) while the negative band at 246 nm remains practically unchanged. The overall changes in the CD spectra indicate the existence of a B → A CT DNA transition that can be attributed to intrastrand linking of adjacent

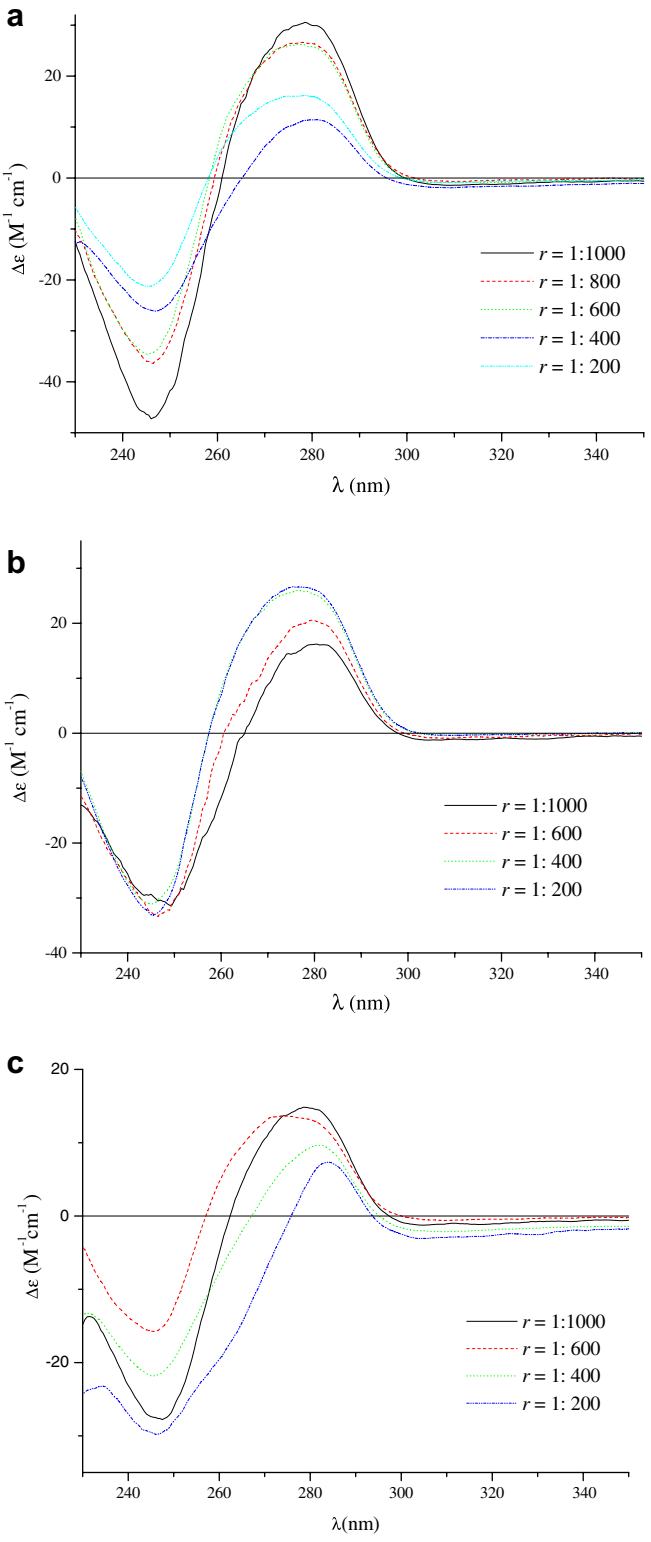

Fig. 5. CD spectra of CT DNA in 5 mM buffer (containing 150 mM NaCl and 15 mM trisodium citrate at pH 7.0) in the presence of: (a) complex $VO(PPA)_2(H_2O)$ (**1**), (b) complex $Mn(PPA)_2(H_2O)_2$ (**2**) and (c) complex $UO_2(PPA)_2$ (**9**), with different r values. The spectra were recorded at 25 °C after samples had been incubated with CT DNA for 24 h at 37 °C.

guanines so that the DNA conformation is modified and destacking of the adjacent bases occurs [81–83]. Similar behavior is observed in the CD spectra of CT DNA in the presence of complexes $Fe(PPA)_3$, $Co(PPA)_2(H_2O)_2$, $Ni(PPA)_2(H_2O)_2$, $Zn(PPA)_2(H_2O)_2$ and $Cd(PPA)_2(H_2O)_2$.

The CD spectra of CT DNA in the presence of complex $UO_2(PPA)_2$ (**9**) are shown in Fig. 5c. The λ_{max} of positive band I is shifted from 275 nm to higher wavelengths (up to 285 nm) followed by a decrease in the intensity upon increase of r, while the intensity of the negative band II at 246 nm increases indicating that the DNA-form changes from the B- to A-form (B → A transition) [81].

4. Conclusions

The synthesis and characterization of nine mononuclear complexes of the first-generation quinolone antibacterial drug pipemidic acid with the ions VO^{2+}, Mn^{2+}, Fe^{3+}, Co^{2+}, Ni^{2+}, Zn^{2+}, MoO_2^{2+}, Cd^{2+} and UO_2^{2+} has been realized with physicochemical and spectroscopic methods. In all the complexes, the pipemidato ligand is bound to the metal via the pyridone oxygen and one carboxylate oxygen atom. Each metal is six-coordinate and its environment could be described as a distorted octahedron. With the use of molecular modelling, we have proposed a low energy model for the structures of $Fe(PPA)_3$, $VO(PPA)_2(H_2O)$ and $MoO_2(PPA)_2$. The antimicrobial activity of the complexes has been tested on three different microorganisms. The complexes show diverse biological activity in comparison to the free pipemidic acid. The best inhibition of the complexes is provided by $UO_2(PPA)_2$ ($MIC = 8\ \mu g\ mL^{-1}$) against the three microorganisms tested. The investigation of the interaction of the complexes with CT DNA has been performed with diverse spectroscopic techniques and showed that the complexes can be bound to CT DNA. For all the complexes, a B → A CT DNA transition has been observed.

Acknowledgements

The authors are grateful to E.L.K.E (70/4/6495) and the "Excellence in the Research Institutes" Program (Action 3.3.1 co-funded by the Greek Ministry of Development and E.U.) for financial support. We thank Prof. M.P. Hendrich, Department of Chemistry, Carnegie Melon University, Pittsburgh, USA for providing us with the EPR simulation program and Dr. I. Eskioglou, Department of Medical Laboratories, Technological and Educational Institution of Larissa, Larissa, Greece for the supply of the microorganisms.

Appendix A. Supplementary material

IR and UV–Vis spectral data for HPPA and all the complexes and ^1H NMR chemical shifts for HPPA, $MoO_2(PPA)_2$ and $UO_2(PPA)_2$. Three schemes (Schemes S1–S3) for the diastereoisomers of $Fe(PPA)_3$, $VO(PPA)_2(H_2O)$ and $MoO_2(PPA)_2$ employed in the simulated annealing calculations. Three Tables (Table S1, S3, and S5)

for the metal–ligand distance restraints applied during the energy minimization phase in order to adjust the geometry of $Fe(PPA)_3$, $VO(PPA)_2(H_2O)$ and $MoO_2(PPA)_2$ models. Three Tables (Table S2, S4, and S6) for the energy statistics from the simulated annealing results of $Fe(PPA)_3$, $VO(PPA)_2(H_2O)$ and $MoO_2(PPA)_2$ diastereoisomers, respectively. Three figures (Figs. S1–S3) for the lowest energy models of $[Fe(PPA)_3]$, $VO(PPA)_2(H_2O)$ and $MoO_2(PPA)_2$ enantiomers. One figure (Fig. S4) for representative UV spectra of all the complexes with CT DNA. Supplementary data associated with this article can be found, in the online version, at doi:10.1016/j.poly.2006.10.017.

References

[1] A. Albert, The Physico-Chemical Basis of Therapy: Selective Toxicity, 6th ed., Chapman & Hall, London, 1979.
[2] M.N. Hughes (Ed.), The Inorganic Chemistry of Biological Processes, 2nd ed., Wiley, New York, 1981.
[3] J. Liu, E.B. Wang, J. Peng, Y.S. Zhou, J. Rare Earths 17 (1999) 139.
[4] S. Chakrabarti, D. Dasgupta, D. Bhattacharyya, J. Biol. Phys. 26 (2000) 203.
[5] I. Turel, Coord. Chem. Rev. 232 (2002) 27.
[6] D. Rehder, J. Costa Pessoa, C.F.G.C. Geraldes, T. Kabanos, T. Kiss, B. Meier, G. Micera, L. Pettersson, M. Rangel, A. Salifoglou, I. Turel, D. Wang, J. Biol. Inorg. Chem. 7 (2002) 384.
[7] S.C. Wallis, L.R. Gahan, B.G. Charles, T.W. Hambley, Polyhedron 14 (1995) 2835.
[8] I. Turel, I. Leban, N. Bukovec, J. Inorg. Biochem. 56 (1994) 273.
[9] I. Turel, L. Golic, O.L. Ruiz Ramirez, Acta Chim. Slov. 46 (1999) 203.
[10] C. Chulvi, M.C. Munoz, L. Perello, R. Ortiz, M.I. Arriortua, J. Via, K. Urtiaga, J.M. Amigo, L.E. Ochando, J. Inorg. Biochem. 42 (1991) 133.
[11] M. Ruiz, R. Ortiz, L. Perello, A. Castineiras, M. Quiros, Inorg. Chim. Acta 211 (1993) 133.
[12] M. Ruiz, R. Ortiz, L. Perello, J. Latorre, J. Server-Carrio, J. Inorg. Biochem. 65 (1997) 87.
[13] M. Ruiz, L. Perello, R. Ortiz, A. Castineiras, C. Maichle-Mossmer, E. Canton, J. Inorg. Biochem. 59 (1995) 801.
[14] M. Ruiz, R. Ortiz, L. Perello, S. Garcia-Granda, M.R. Diaz, Inorg. Chim. Acta 217 (1994) 149.
[15] M. Ruiz, L. Perello, J. Server-Carrio, R. Ortiz, S. Garcia-Granda, M.R. Diaz, E. Canton, J. Inorg. Biochem. 69 (1998) 231.
[16] A. Koppenhofer, U. Hartmann, H. Vahrenkamp, Chem. Ber. 128 (1995) 779.
[17] B. Macias, M.V. Villa, I. Rubio, A. Castineiras, J. Borras, J. Inorg. Biochem. 84 (2001) 163.
[18] Z.-F. Chen, R.-G. Xiong, J. Zhang, X.-T. Chen, Z.-L. Xue, X.-Z. You, Inorg. Chem. 40 (2001) 4075.
[19] G. Mendoza-Diaz, L.M.R. Martinez-Aguilera, R. Perez-Alonso, Inorg. Chim. Acta 138 (1987) 41.
[20] G. Mendoza-Diaz, L.M.R. Martinez-Aguilera, R. Moreno-Esparza, K.H. Pannell, F. Cervantes-Lee, J. Inorg. Biochem. 50 (1993) 65.
[21] S.C. Wallis, L.R. Gahan, B.G. Charles, T.W. Hambley, P.A. Duckworth, J. Inorg. Biochem. 62 (1996) 1.
[22] I. Turel, K. Gruber, I. Leban, N. Bukovec, J. Inorg. Biochem. 61 (1996) 197.
[23] Z.-F. Chen, B.-Q. Li, Y.-R. Xie, R.-G. Xiong, X.-Z. You, X.-L. Feng, Inorg. Chem. Commun. 4 (2001) 346.
[24] L.Z. Wang, Z.F. Chen, Z.S. Wang, H.Y. Li, R.G. Xiong, X.Z. You, Chin. J. Inorg. Chem. 18 (2002) 1185.
[25] D.J. Wang, Z.D. Fang, D.Y. Han, Chem. Res. Chin. Univ. 21 (2005) 258.
[26] E.I. Steifel, in: G. Wilkinson (Ed.), Comprehensive Coordination Chemistry, vol. 3, Pergamon Press, Oxford, 1989, pp. 1375–1420.
[27] P. Testillano, M. Sanchez-Pina, A. Olmedilla, M. Ollacarizqueta, C. Tandler, M. Risueno, J. Histochem. Cytochem. 39 (1991) 1427.
[28] P.E. Nielsen, C. Hiort, S.H. Sonnichsen, O. Buchardt, O. Dahl, B. Norden, J. Am. Chem. Soc. 114 (1992) 4967.
[29] A. Papakyriakou, A. Anagnostopoulou, A. Garnier-Suillerot, N. Katsaros, Eur. J. Inorg. Chem. (2002) 1146.
[30] K.G. Naber, J. Antimicrob. Chemother. 46 (2000) 49.
[31] V. Mersch-Sundermann, K.H. Hauff, P. Braun, W. Lu, Int. J. Oncol. 5 (1994) 855.
[32] L. Yang, W. Li, D.L. Tao, Y.F. Li, X.L. Yang, Synth. React. Inorg. Met.-Org. Chem. 29 (1999) 1485.
[33] L. Yang, D. Tao, X. Yang, Y. Li, Y. Guo, Chem. Pharm. Bull. 51 (2003) 494.
[34] B. Szymanska, D. Skrzypek, D. Kovala-Demertzi, M. Staninska, M.A. Demertzis, Spectrochim. Acta A 63 (2006) 518.
[35] B. Qiao, Y. Lu, C. Xuan, Chem. Res. Chin. Univ. 10 (1994) 341.
[36] E.K. Efthimiadou, Y. Sanakis, M. Katsarou, C.P. Raptopoulou, A. Karaliota, N. Katsaros, G. Psomas, J. Inorg. Biochem. 100 (2006) 1378.
[37] E.K. Efthimiadou, Y. Sanakis, C.P. Raptopoulou, A. Karaliota, N. Katsaros, G. Psomas, Bioorg. Med. Chem. Lett. 16 (2006) 3864.
[38] G. Psomas, A. Tarushi, E.K. Efthimiadou, Y. Sanakis, C.P. Raptopoulou, N. Katsaros, J. Inorg. Biochem. 100 (2006) 1764.
[39] E.K. Efthimiadou, H. Thomadaki, Y. Sanakis, C.P. Raptopoulou, N. Katsaros, A. Scorilas, A. Karaliota, G. Psomas, J. Inorg. Biochem. (2006) (doi: doi:10.1016/j.jinorgbio.2006.07.019).
[40] E. Tselepi-Kalouli, N. Katsaros, J. Inorg. Biochem. 37 (1989) 271.
[41] A.P. Golombek, M.P. Hendrich, J. Magn. Reson. 165 (2003) 33.
[42] A.K. Upadhyay, A.B. Hooper, M.P. Hendrich, J. Am. Chem. Soc. 128 (2006) 4330.
[43] N.L. Allinger, J. Am. Chem. Soc. 99 (1977) 8127.
[44] P. Christofis, M. Katsarou, A. Papakyriakou, Y. Sanakis, N. Katsaros, G. Psomas, J. Inorg. Biochem. 99 (2005) 2197 (and references therein).
[45] I. Turel, A. Golobic, A. Klavzar, B. Pihlar, P. Buglyo, E. Tolis, D. Rehder, K. Sepcic, J. Inorg. Biochem. 95 (2003) 199.
[46] I. Correia, J. Costa Pessoa, M.T. Duarte, R.T. Henriques, M.F.M. Piedade, L.F. Veiros, T. Jakusch, T. Kiss, A. Dornyei, M.M.C.A. Castro, C.F.G.C. Geraldes, F. Avecilla, Chem. Eur. J. 10 (2004) 2301.
[47] S.S. Amin, K. Cryer, B. Zhang, S.K. Dutta, S.S. Eaton, O.P. Anderson, S.M. Miller, B.A. Reul, S.M. Brichard, D.C. Crans, Inorg. Chem. 39 (2000) 406.
[48] J. Costa Pessoa, I. Cavaco, I. Correia, I. Tomaz, T. Duarte, P.M. Matias, J. Inorg. Biochem. 80 (2000) 35.
[49] M. Scarpellini, A. Neves, A.J. Bortoluzzi, I. Vencato, V. Drago, W.A. Ortiz, C. Zucco, J. Chem. Soc., Dalton Trans. (2001) 2616.
[50] L. Westerheide, F.K. Muller, R. Than, B. Krebs, J. Dietrich, S. Schindler, Inorg. Chem. 40 (2001) 1951.
[51] J.M. Rowland, M. Olmstead, P.K. Mascharak, Inorg. Chem. 40 (2001) 2810.
[52] K. Matsumoto, T. Ozawa, K. Jitsukawa, H. Einaga, H. Masuda, Inorg. Chem. 40 (2001) 190.
[53] E.J. Brown, A.C. Whitwood, P.H. Walton, A.-K. Duhme-Klair, J. Chem. Soc., Dalton Trans. (2004) 2458.
[54] Z.-H. Zhou, S.-Y. Hou, Z.-X. Cao, H.-L. Wan, S.-W. Ng, J. Inorg. Biochem. 98 (2004) 1037.
[55] S.-M. Chen, C.-Z. Lu, Y.-Q. Yu, Q.-Z. Zhang, X. He, Acta Crystallogr., Sect. C 60 (2004) m437.
[56] A.-K. Duhme-Klair, G. Vollmer, C. Mars, R. Frohlich, Angew. Chem., Int. Ed. 39 (2000) 1626.
[57] M.P. Allen, D.J. Tildesley (Eds.), Computer Simulation of Liquids, Oxford University Press, Oxford, 1989.
[58] C. Dendrinou-Samara, G. Tsotsou, C.P. Raptopoulou, A. Kortsaris, D. Kyriakidis, D.P. Kessissoglou, J. Inorg. Biochem. 71 (1998) 171.

[59] K. Nakamoto, Infrared and Raman Spectra of Inorganic and Coordination Compounds, 4th ed., Wiley, New York, 1986.
[60] G.B. Deacon, R.J. Phillips, Coord. Chem. Rev. 33 (1980) 227.
[61] E.J. Tolis, V.I. Teberekidis, C.P. Raptopoulou, A. Terzis, M.P. Sigalas, Y. Deligiannakis, T.A. Kabanos, Chem. Eur. J. 7 (2001) 2698.
[62] E. Garribba, G. Micera, A. Panzanelli, D. Sanna, Inorg. Chem. 42 (2003) 3981.
[63] H. Kelm, H.-J. Kruger, Inorg. Chem. 35 (1996) 3533.
[64] M. Nakai, M. Obata, F. Sekiguchi, M. Kato, M. Shiro, A. Ichimura, I. Kinoshita, M. Mikuriya, T. Inohara, K. Kawabe, H. Sakurai, C. Orvig, S. Yano, J. Inorg. Biochem. 98 (2004) 105.
[65] W.O. Koch, V. Schunemann, M. Gerdan, A.X. Trautwein, H.-J. Krüger, Chem. Eur. J. 4 (1998) 1255.
[66] H. Chun, C.N. Verani, P. Chaudhuri, E. Bothe, E. Bill, T. Weyhermuller, K. Wieghardt, Inorg. Chem. 40 (2001) 4157.
[67] D.A. Buckingham, C.R. Clark, in: G. Wilkinson (Ed.), Comprehensive Coordination Chemistry, vol. 4, Pergamon Press, Oxford, 1989, pp. 635–900.
[68] L. Sacconi, F. Mani, A. Bencini, in: G. Wilkinson (Ed.), Comprehensive Coordination Chemistry, vol. 5, Pergamon Press, Oxford, 1989, pp. 1–347.
[69] M. Sakai, A. Hara, S. Anjo, M. Nakamura, J. Pharm. Biomed. Anal. 18 (1999) 1057.
[70] N.D. Chasteen (Ed.), Biological Magnetic Resonance, Plenum, New York, 1981, pp. 53–119 (Chapter 2).
[71] T.S. Smith, R. LoBrutto, V.L. Pecoraro, Coord. Chem. Rev. 228 (2002) 1 (and references therein).
[72] T.S. Smith, C.A. Root, J.W. Kampf, P.G. Rasmussen, V.L. Pecoraro, J. Am. Chem. Soc. 122 (2000) 767.
[73] A.D. Russell, in: S.S. Block (Ed.), Disinfection, Sterilization and Preservation, 4th ed., Lea & Febiger, Philadelphia, PA, 1991, pp. 27–59.
[74] H.W. Rossmore, in: S.S. Block (Ed.), Disinfection, Sterilization and Preservation, 4th ed., Lea & Febiger, Philadelphia, PA, 1991, pp. 290–321.
[75] A. Rodger, B. Norden (Eds.), Circular Dichroism and Linear Dichroism, Oxford University Press, Oxford, 1997.
[76] G. Song, Y. He, Z. Cai, J. Fluoresc. 14 (2004) 705.
[77] P. Drevensek, I. Turel, N.P. Ulrih, J. Inorg. Biochem. 96 (2003) 407.
[78] G.S. Son, J-.A. Yeo, M.-S. Kim, S.K. Kim, A. Holmen, B. Akerman, B. Norden, J. Am. Chem. Soc. 120 (1998) 6451.
[79] W. Curtis-Johnson, in: K. Nakanishi, N. Berova, R.W. Woody (Eds.), CD of Nucleic Acids in Circural Dichroism, Principles and Applications, VHS, New York, 1994, pp. 523–540.
[80] C.K.S. Pillai, U.S. Nandi, Biochim. Biophys. Acta 474 (1977) 11.
[81] N. Nikolis, C. Methenitis, G. Pneumatikakis, J. Inorg. Biochem. 95 (2003) 177.
[82] T.C. McGregor, Z. Balcharova, Y. Qu, M.-C. Tran, R. Zadulova, V. Brabec, N. Farrel, J. Inorg. Biochem. 77 (1999) 43.
[83] T.C. Jenkins, in: K.R. Fox (Ed.), Drug–DNA Interaction Protocols, Humana Press, Totowa, NJ, 1997, pp. 195–218.